Chemical Engineering Science 207 (2019) 769–779

Contents lists available at ScienceDirect

Chemical Engineering Science

journal homepage: www.elsevier.com/locate/ces

Continuum-scale modeling of water infiltration into a stack of two thin fibrous layers and their inter-layer space

Amir Hossein Tavangarrad [a,*], Behzad Mohebbi [b,c], Chaozhong Qin [d], S. Majid Hassanizadeh [a], Rodrigo Rosati [b], Jan Claussen [b], Bernhard Blümich [c]

[a] Department of Earth Sciences, Environmental Hydrogeology Group, Utrecht University, Princetonlaan 8a, 3584CB Utrecht, the Netherlands
[b] Procter&Gamble Service GmbH, Sulzbacher Str. 40, 65824 Schwalbach am Taunus, Germany
[c] Institut für Technische und Makromolekulare Chemie, RWTH Aachen, D-52056, Germany
[d] Department of Mechanical Engineering, Eindhoven University of Technology, the Netherlands

HIGHLIGHTS

- Richards model fails in predicting water infiltration into a stack of two thin fibrous layers.
- Reduced continua model (RCM) can reproduce our NMR experimental results.
- RCM is much more computational efficient than Richards model.

ARTICLE INFO

Article history:
Received 30 March 2019
Received in revised form 28 June 2019
Accepted 1 July 2019
Available online 5 July 2019

Keywords:
Thin porous media
Liquid infiltration
Low-field NMR
Fibrous layer
Richards model
Reduced Continua Model

ABSTRACT

Unsaturated water flow through thin porous layers plays an important role in many applications such as water management in hydrogen fuel cells and hygiene products. It is well known that void spaces between adjacent thin layers (i.e., layer-layer interfaces) considerably impact through-plane water infiltration. Therefore, it is essential to account for this fact in the model development. Recently, we reported Nuclear Magnetic Resonance (NMR) measurements of water infiltration into a stack of two thin porous layers of 43-gsm polyester and showed crucial effect of the inter-layer space on the transfer of liquid from one layer to the other. In this work, we aim to test two numerical models of water infiltration into two (partially dry) thin porous layers. One is the standard Richards model for unsaturated flow and the other is Reduced Continua Model (RCM). The latter model is based on thickness-averaged properties and does not provide through-plane distribution of saturation in the layers. Layer-scale material properties are experimentally measured. Sub-layer material properties, which are used in the Richards model, are obtained by pore-morphology modeling of micro-CT images. Our results show that the RCM is superior to the Richards model. It can predict NMR measurements of temporal evolutions of water contents in the two layers quite well. Moreover, it is computationally much more efficient.

1. Introduction

Stacked thin fibrous layers are encountered in many applications, such as, hygiene products (Diersch et al., 2011), polymer electrolyte fuel cells (Qin and Hassanizadeh, 2015, Carrere and Prat, 2019, Qin et al., 2019) and many other productions (Albrecht et al., 2003; Prat and Agaësse, 2015). Knowledge of water flow through those thin layers and across their layer-layer interface is of great importance for understanding and predicting their performance. Although a thin fibrous layer usually has only a few (10 to 15) pores along its thickness, it is highly porous. Therefore, it is difficult to define a representative elementary volume (REV) along the thickness (Qin and Hassanizadeh, 2014). Most thin fibrous layers are soft and their pore structure can change considerably under compression (Leisen et al., 2009). Furthermore, the inter-layer condition strongly depends on compression. The inter-layer condition could dominate mass exchange between layers. Additionally, a clear layer boundary between neighboring layers cannot be identified easily in a stack of fibrous layers. These factors have given rise to many challenges in characterizing and modeling thin fibrous layers.

* Corresponding author at: Department of Earth Sciences, Environmental Hydrogeology Group, Utrecht University, Princetonlaan 8a, 3584CB Utrecht, the Netherlands.
E-mail address: A.H.Tavangarrad@uu.nl (A.H. Tavangarrad).

https://doi.org/10.1016/j.ces.2019.07.001
0009-2509/

In continuum scale modeling, a thin fibrous layer is commonly discretized into a three-dimensional (3D) computational grid, on which 3D flow equations are solved. In this approach, the thin porous layer is assumed to be homogeneous in the through-plane direction. However, there are several problems with this methodology, such as the failure of the representative elementary volume (REV) concept (Garcia-Salaberri et al., 2019), heavy computational efforts (Hao et al., 2016), and the neglect of the layer-layer interfacial effect (Hizir et al., 2010). Since REV cannot be defined for thin fibrous layers, it is difficult to obtain the distribution of "macroscopic" material properties over the thickness and ambiguity arises in interpretation of modeling results. Moreover, for thin layers, with lateral dimensions much larger than their thickness, discretization of the modeling domain leads to high mesh density and accordingly high computational effort. Besides, in multilayer structures, the layer-layer interface could dominate the flow and it is unclear how to incorporate this effect into macroscale equations.

The effect of the inter-layer pore space on continuum-scale modeling of unsaturated fluid flow in stacked thin fibrous layers has not received enough attention up to now [Hizir et al., 2010]. To illustrate the concept of inter-layer space, side-view images of fibers of two adjacent thin fibrous layers, obtained with micro-CT (μCT) scanner, are shown in Fig. 1. The gap between two layers is referred to as the inter-layer space, or interface region, that can be distinguished from the two layers in the enlarged section of the image. Prat and Agaësse (2015) proposed the concept of a third layer that is the transition region forming the interface between the neighboring layers. They used a pore-network model to investigate influence of the interface morphology on fluid invasion patterns in a two-layer porous system. They found that at equilibrium, a completely different liquid distribution is established in a two-layer system with a large single pore in the inter-layer space compared to the system with a collection of pores between the two layers. The third layer concept can be implemented in the traditional continuum scale modeling as an additional layer between two thin layers. However, determining the hydraulic properties of a virtual third layer introduces additional complexity. Not only the REV concept does not hold for such an interface, but also the virtual third layer thickness cannot be clearly identified. Also, its macroscale properties should be artificially defined.

To resolve the above-mentioned shortcomings, Qin and Hassanizadeh (2014) reformulated the governing equations of multiphase flow and solute transport for a stack of thin fibrous layers. A new model called Reduced Continua Model (RCM) has been developed in which thin porous layers are treated as a number of 2D continua. Macroscale balance laws are formulated in terms of thickness-averaged properties, which are experimentally measurable. The exchanges of mass, momentum, and energy between two adjacent layers, through the inter-layer space, are modeled explicitly.

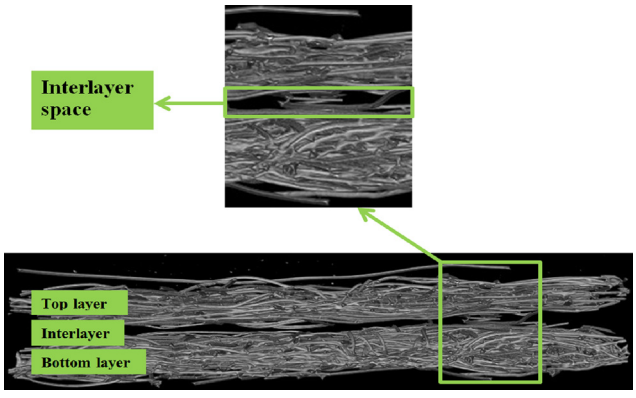

Fig. 1. μCT images of two 43-gsm layers on top of each other without compression.

The RCM approach can account for the presence of the inter-layer region in a robust fashion. Its effect is modelled by means of terms for exchange of mass, momentum and energy between the two layers [Qin and Hassanizadeh, 2014]. The mass exchange term is assumed to be linearly dependent on the pressure difference between two adjacent layers. Furthermore, the mass transfer coefficient appearing in the RCM is assumed to depend on saturations as well as the material properties of the two layers. This function is very similar to the concept of relative permeability and therefore was linked to saturations of neighboring layers (Qin and Hassanizadeh, 2015; Tavangarrad et al., 2018). In general, this function should be determined by laboratory experiments.

In a previous study, we applied the RCM to the modeling of liquid transfer from a fully saturated thin layer to a dry layer of identical material (Tavangarrad et al., 2018). The advantages of the RCM were demonstrated, in terms of both the treatment of the layer-layer interface and the computational efficiency. However, in that work, a very small liquid redistribution occurred and the saturation range was limited. Furthermore, the saturation distribution profile over the thickness was not measured; so, distribution of saturation along the thickness was not provided. In this study, we employ the RCM to simulate an experiment with a wide range of saturation changes and detailed information about the water distribution over the thickness of the layers.

The main objective of this study is to test both traditional Richards model and the RCM against experimental data obtained in our previous work (Mohebbi et al., 2018) on through-plane liquid infiltration in a stack of two thin fibrous layers. In those experiments, water was fed at a small region in the middle of the top layer. Liquid ingress through the two thin fibrous layers and their interface was observed over time. Additionally, one of our research objectives is to characterize the thin fibrous layers and determine their material properties numerically.

This paper is organized as follows. We start with describing the measurement method, the experimental results, and the materials used in our previous work (Mohebbi et al., 2018) in Section 2. Next, in Section 2.3, we describe the characterization of the thin fibrous layers, and obtain properties that are used in the modeling study. The analysis of μCT images from the stack of two layers is also presented in this section. We also show the effect of compression on the pore structure of the stack of two layers and their interface. Additionally, the measured hydraulic properties of a single layer and a stack of two layers are compared with the results of the pore morphology simulation method. In Section 3, two continuum-scale modeling approaches, the RCM and the Richards model, are introduced briefly. Results of both modeling techniques are presented and compared to measurement data in Section 4, which is followed by conclusions in Section 5.

2. Materials, experiments, and characterization approaches

2.1. Materials

In our experiments, spunbonded non-woven fibrous layers were used, under 0.3 psi (≅2.1 kPa) compression. Layers were produced in a similar way from polyethylene terephthalate (polyester) fibers. The areal mass density of each fabric is 43 g per square meter (gsm), and its porosity is around 0.89. The properties of the 43-gsm polyester layer under 0.3 psi compression are given in Table 1. A specific surfactant has been added to this material to make it hydrophilic.

Table 1
Properties of a compressed single 43-gsm polyethylene terephthalate (polyester) fibrous layer used in this study.

Fiber density [g/cm^3]	Porosity [-]	Fiber radius [μm]	VG formula α[1/Pa]	VG formula n[-]	Thickness [μm]
1.36	0.89	16	0.00197	4.8	310

2.2. NMR experiments

In our previous study (Mohebbi et al., 2018), two square thin polyester layer samples with dimension of 10 by 10 mm^2 were placed on top of each other. A Plexiglas plate with a hole in the center was placed on the upper layer in order to impose a pressure of 0.3 psi (≅2.1 kPa) as shown in Fig. 2. The stack of two layers is about 640 μm thick under compression. The hole had a diameter of 1 mm. It was used for delivering a saline solution (consisting of 0.9%wt NaCl and distilled water) at a constant rate to the top layer using a syringe pump. Two different experiments were performed: (i) high flow rate of 30 μl/min for 60 s, (ii) low flow rate of 11.4 μl/min for 160 s.

Detailed description of the experiments was presented in Mohebbi et al., 2018. Here, we provide a short description of the experiments and present results of the high flow rate experiment (Adopted from Mohebbi et al., 2018). Additionally, signal intensity profiles of high flow rate experiment at a large number of times and results of the low flow rate experiment are given here for the first time.

The distributions of the saline solution over the thickness of the layers and their variations with time were determined from images obtained using a mobile single-sided nuclear magnetic resonance (NMR) instrument. The measurement aperture of the NMR instrument had a thickness of 44 μm over the whole layer area. In other words, the signal was averaged over a volume of 10 mm × 10 mm × 44 μm. Results are shown in Fig. 3. At any given time, there are 15 data points, each assigned to the center of 44-μm slice. The amplitude of the NMR signal was assumed to be linearly proportional to the liquid content (Mohebbi et al., 2019). As revealed in Fig. 3, the interface region between the layers has a lower amount of liquid compared to the two layers. Based on signal intensity profiles at different times, we can identify three different phases of the water infiltration process. In the first phase, which takes 12 s, water accumulates in the top layer only, with no water entering the interface region and the bottom layer. In the second phase, until about 24 s, while the water content remains very low in the interface region (centered around 340 μm through the thickness), the water saturation increases in the bottom layer. In the last phase, more water pathways are created in the inter-layer space, water accumulates in this region too as equilibrium in the two layers is approached.

We calculated the average saturation of each layer based on a calibration of the signals acquired from all slices of a layer and its porosity. Obviously, the average saturations of top and bottom layers increase with time, as shown in Fig. 4a. For the high flow rate experiment, the results displayed in this figure show that time lag of saturation buildup in the lower layer is more than 11 s. For the experiments with the lower flow rate of 11.4 μl/min, the time lag was much larger, as expected (Fig. 4b). This is because it takes longer for the saturation buildup in the upper layer, before the inter-layer space can be invaded, due to the low flow rate. Note that the experimental data are scattered more in the low flow-rate experiment. This artifact can be attributed to the large

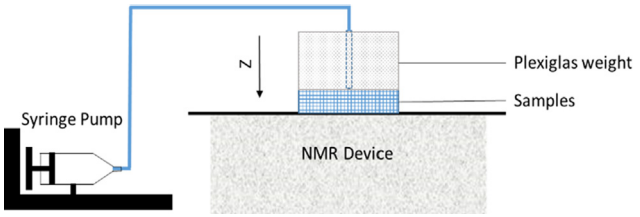

Fig. 2. Sketch of the experimental setup (Mohebbi et al., 2018).

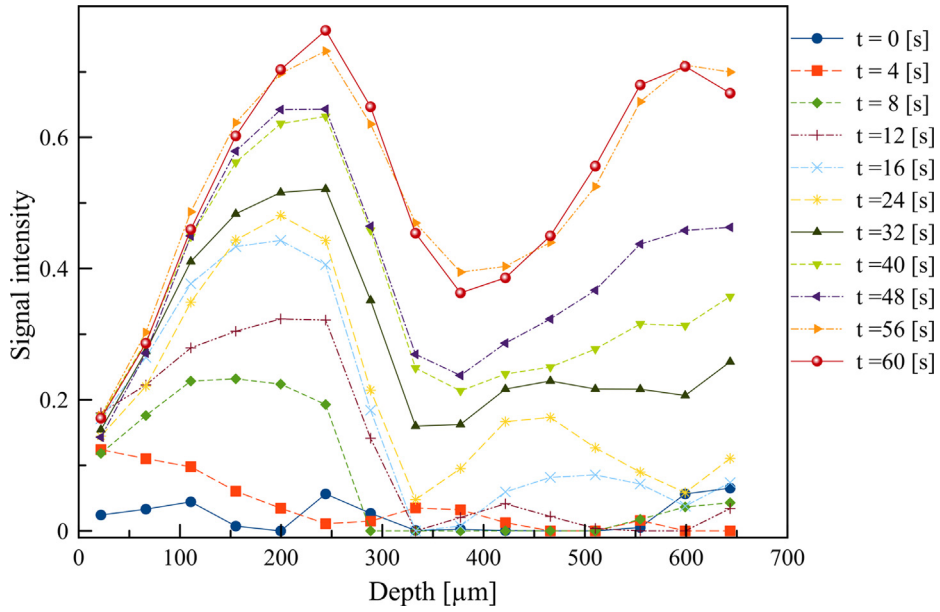

Fig. 3. Temporal evolution of signal profiles over the thickness of a stack of two polyester layers obtained from NMR measurements when a constant flow rate of 30 μl/min was applied for 60 s (adopted from Mohebbi et al., 2018).

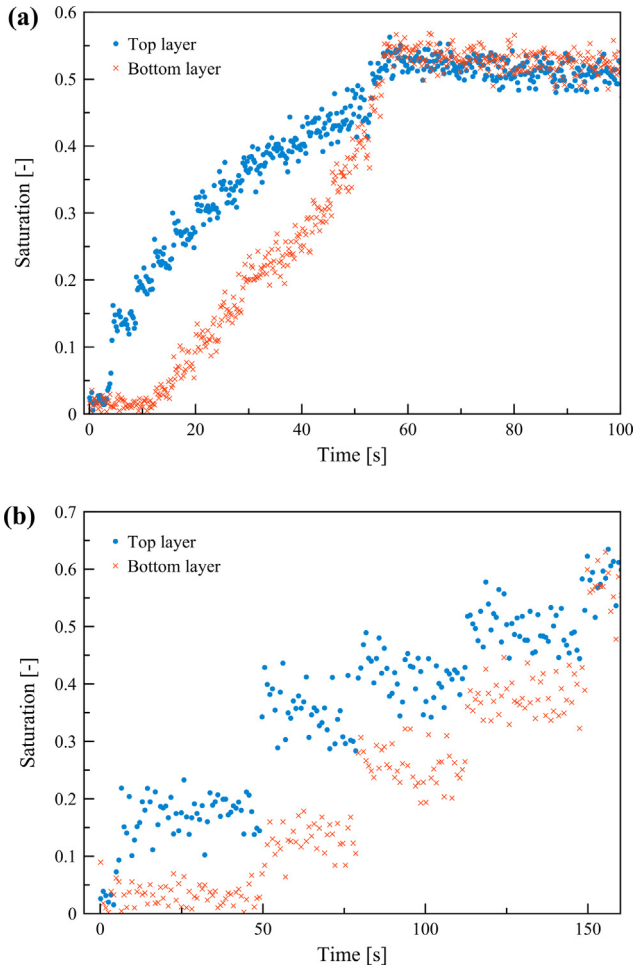

Fig. 4. Evolution of the average saturation of each layer over time obtained from NMR measurements in two different experiments: (a) a constant flow rate of 30 μl/min applied for 60 s (adopted from Mohebbi et al., 2018), and (b) a constant flow rate of 11.4 μl/min applied for 160 s.

dispersion of the data and the so called stair-step effect due to the slow change of saturation.

It was qualitatively shown in previous studies on woven fibrous materials (Zhuang et al., 2002) that a saturation-build-up threshold can be defined for the layer-layer mass exchange. Zhuang et al., (2002) stated that this threshold is smaller for a larger compression. Similarly, Birrfelder et al. (2013) observed longer time delays for water movement from one woven layer to its identical layer when the compression decreased. Among other factors, the saturation-build-up threshold depends on the entry pressure of the interface region between the layers. In other words, the nature of the interface region imposes a minimum limit for liquid saturation in the top layer before entering the bottom layer.

From results shown in Fig. 4, we can see that the saturation threshold for the combination of two 43-gsm polyester layers, compressed under 0.3 psi (≅2.1 kPa) pressure, is approximately 0.25. The connectivity of the two layers is also a critical factor for liquid transport in the interface region. For instance, our experimental result of water injection into two polyester layers without compression (not presented here) showed that the liquid did not enter bottom layer at all, because only few connection points existed between the two layers. This can be seen in the image of two polyester layers without compression, shown in Fig. 1. The experimental results summarized in this section are evidence of the role of the interface region on the transfer of liquid from the upper to the lower layer.

2.3. Characterization approaches

The pore structure of the two layers, with and without compression, was obtained from images acquired with a μCT scanner (Scanco μCT50) with an isotropic voxel resolution of four microns. The μCT images were imported into ImageJ software for thresholding and noise filtration. First, we segmented the gray scale images by setting meaningful thresholds in order to eliminate shadows artifact in all images. Then, we used median filter to filter out the isolated voxels smaller than the fiber radius. Fig. 5 shows the top view of a $4 \times 4\ mm^2$ section of the stack of two layers after image processing. The dashed red circle shows one of the bonding points where fibers are pressed together during the production process. Bonding points are distributed all over the layer in a regular pattern. In Fig. 6, the layer-layer interface can be seen in a cross-sectional view of a stack of two layers with and without compression. We see a large gap between the two layers in the uncompressed case (Fig. 6a). Imposing 0.3 psi (≅2.1 kPa) pressure causes the gap to close significantly, as seen in Fig. 6b. The pronounced differences between the compressed and the uncompressed cases are evident in the 2D binary images (Fig. 6c and d). However, there are still large pores in the interface region even after compression (Fig. 6d).

The variation of the fiber content across the layers thickness was determined using a MATLAB code developed in-house, with binary images used as an input. Results (see Fig. 7) shows that the fiber content varies non-uniformly along the thickness of the layers. It has a bell shaped form for both layers. The data is used to calculate the variation of porosity over the thickness. As a result of the compression, both porosity and thickness of the stack are reduced.

The thin 43-gsm polyester layer used in this study consists of small pores in its middle regions and larger pores near the surfaces. The bonding points (marked in Fig. 5) contribute to higher fiber content in the middle. The very low fiber content at the surface of each layer corresponds to a few fibers sticking out of the layer. This raises a question about the exact thickness of a thin layer. Among other factors, the nominal thickness of a single layer of fabric depends on the layer surface roughness, fabric wrinkles, and

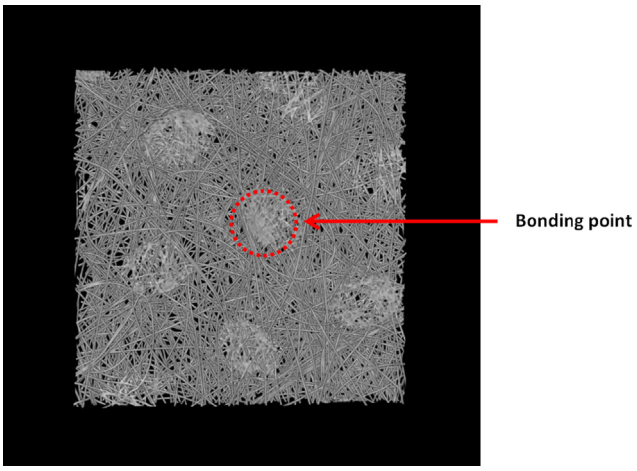

Fig. 5. Top view of a $4 \times 4\ mm^2$ section of a stack of two polyester layers, compressed under 0.3 psi pressure. One of the bonding points is marked with a dashed red circle. (For interpretation of the references to colour in this figure legend, the reader is referred to the web version of this article.)

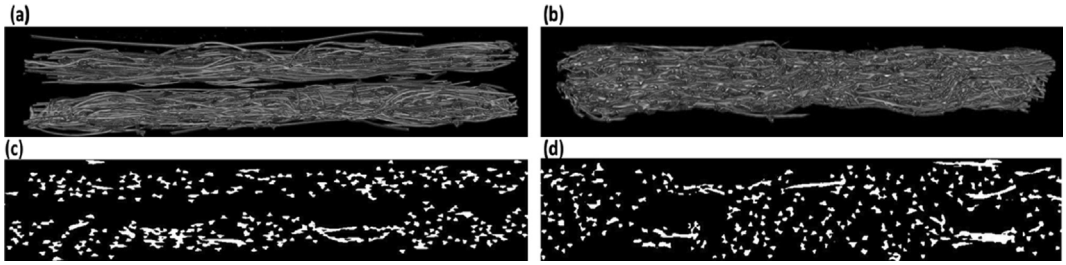

Fig. 6. Side view of a stack of two polyester layers: (a) without compression, (b) under 0.3 psi compression. 2D binary image of the cross sectional cut of the stacked layers: (c) without compression, (d) under 0.3 psi compression.

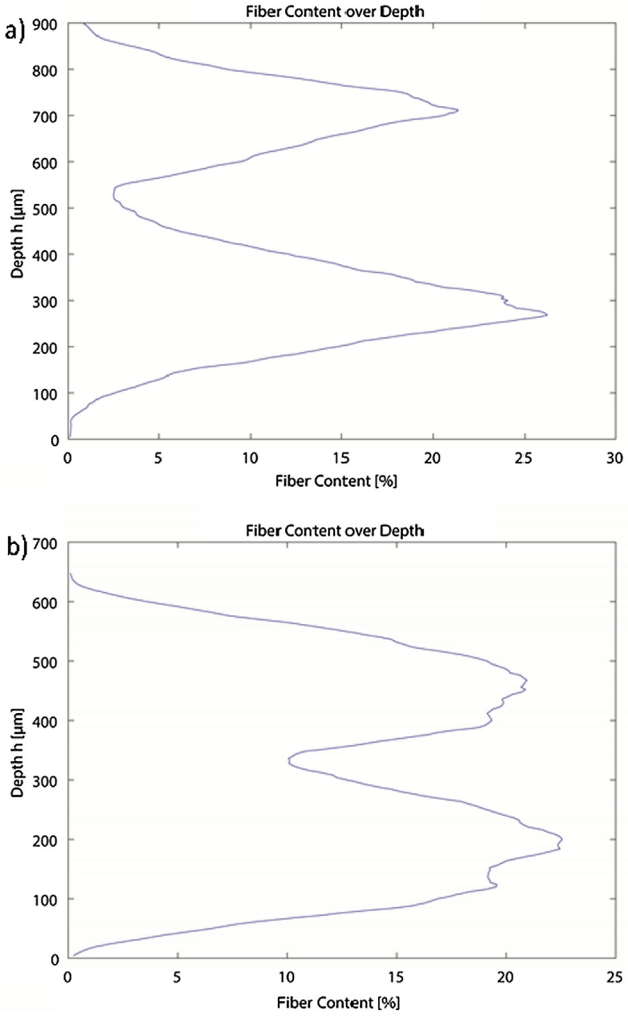

Fig. 7. Fiber content variation over thickness of two polyester layers: (a) without compression, (b) under 0.3 psi compression. Results shown for the layers under compression are adapted from Mohebbi et al., 2018.

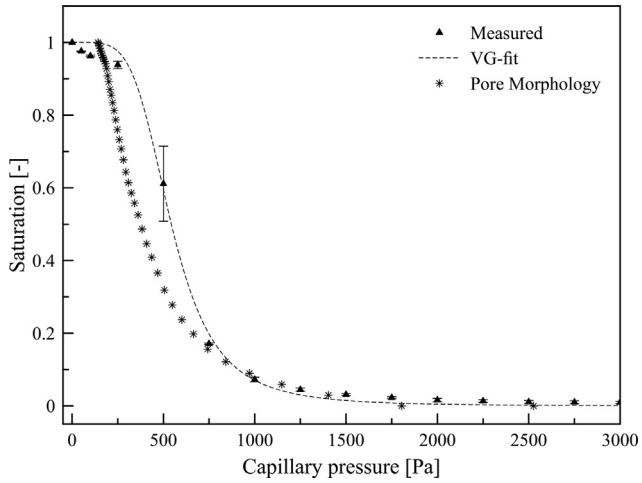

Fig. 8. Measured and calculated imbibition capillary pressure-saturation data for a single compressed polyethylene terephthalate layer. The experimental data points are fitted with the VG formula. The error bars represent the standard deviation from duplicate measurements.

bonding points. One can determine the thickness of two layers from the image analysis results provided in Fig. 7. Assuming the layer surface to start at zero fiber content, the thickness of the two layers is estimated to be 640 μm under compression.

The hydraulic properties of the thin fibrous layers in this study were determined both numerically and experimentally. The capillary pressure-saturation relationship for a single 43-gsm polyester layer was measured with the autoporosimetry technique developed for fibrous layers by Miller and Tomkin (1994). The measurements were performed on a circular piece of a sample with the diameter of 5 cm. Only imbibition experiments were performed. The measured data points were fitted using van Genuchten (1980) formula (Eq. (3)) and results are shown in Fig. 8. The error bars are based on duplicate measurements. Fitting parameters and other measured properties are listed in Table 1. Based on our previous experimental study of the capillary pressure-saturation relationship for thin fibrous layers, doubling the number of layers had little impact on this relationship (Tavangarrad et al., 2019; Tavangarrad, 2019). Clearly, with the current measurement setup, we were not able to characterize the interface region separately. One possible way to obtain the capillary pressure-saturation relationship of the interface region is to combine the single sided low-field NMR device with the autoporosimetry instrument in order to measure the water content variation over the thickness of a stack of layers and their inter-layer space at any given pressure step, at equilibrium. But, this characterization technique is out of the scope of the current study. As an alternative to measurements, we have used the pore morphology simulation method to obtain the capillary pressure-saturation relationship for a single layer, sub-regions of a layer or the interface region between two layers. The pore morphology method is a quasi-static geometric approach that was developed by Hazlet (1995) and improved later by Hilpert and Miller (2001). It has been used for obtaining capillary pressure-saturation relationships for fibrous materials (Tafreshi and Bucher, 2013) and a packing of highly swelling grains (Sweijen et al., 2017).

We employed the pore morphology method to determine the material properties of a stack of two polyester layers based on their μCT images similar to those shown in Fig. 6b. The characterization

of the stack is based on three different modeling approaches. In the first modeling approach, *model 1*, we simulate the two layers as two identical homogeneous domains that are in perfect contact with each other. So, in this case, it is sufficient to find the properties of a single layer only. In *model 2*, the modeling domain is assumed to consist of three homogeneous domains: in addition to the upper and the lower layers, we consider the interface region as a third virtual domain, with properties different from the two layers. In the third approach (*model 3*), the two layers and their interface are divided into 14 different subdomains with equal thicknesses, but each with its own properties. Properties of each sublayer could be determined from μCT images using the pore morphology technique. The main goal is to see how variation of properties along the thickness of two layers can affect the numerical simulation results. Moreover, the measurement results of each sensitive slice can be compared with numerical results. We use all three modeling approaches to provide input for the traditional Richards model while the *model 1* is the only characterization approach employed for the RCM simulations.

A quasi-static imbibition simulation was performed for each modeling subdomain using the pore morphology technique. The top and bottom boundaries of the subdomain were set to be in contact with wetting and non-wetting phase reservoirs, respectively. Properties of fluid phases as well as their surface tension and contact angle with the solid phase were given as input parameters in the Geodict software (Math2Market GmbH). It should be noted that the contact angle was assumed to be 80 degrees and constant in this approach. The surface tension between water and air was considered to be constant and equal to 0.072 N/m.

In *model 1* approach, we divided images of the stack of two layers into two subdomains with equal thickness, representing top and bottom layers. Computed capillary pressure-saturation data points for top and bottom layers are shown in Fig. 9. Also shown in this figure are the pore morphology results for the stack of two layers. The pore morphology method gives similar curves for the top layer, the bottom layer, and the double layers. Consequently, doubling the number of layers did not seem to affect the curves significantly. The computed curve for a single layer is plotted along with the measured curve in Fig. 8. Observed discrepancies between the numerical and experimental results in this case study are due to physical phenomena that are missed in the pore morphology method. For instance, the effect of the surfactant wash-off during imbibition process, and corresponding changes in the surface tension and contact angle, could not be taken into account by the current model. Other hydraulic properties of top and bottom layers are listed in Table 2. Both intrinsic permeability and relative permeability are determined using the Geodict software package. Results of the intrinsic permeability values obtained from solving the Stokes equation are in good agreement with values of the empirical equation of Jackson and James (1986) (Table 2). The calculated relative permeability data points satisfactorily agree with formula suggested by van Genuchten (1980) for relative permeability function (See Appendix A). Hence, we used van Genuchten fitting parameters to specify the relative permeability function in this study. Next, according to *model 2* approach, a virtual third layer with a thickness of 44 μm was cut from the middle part of the stack of images and characterized with the pore morphology method. Results are shown in Fig. 10 and compared with the measured curve for a single layer.

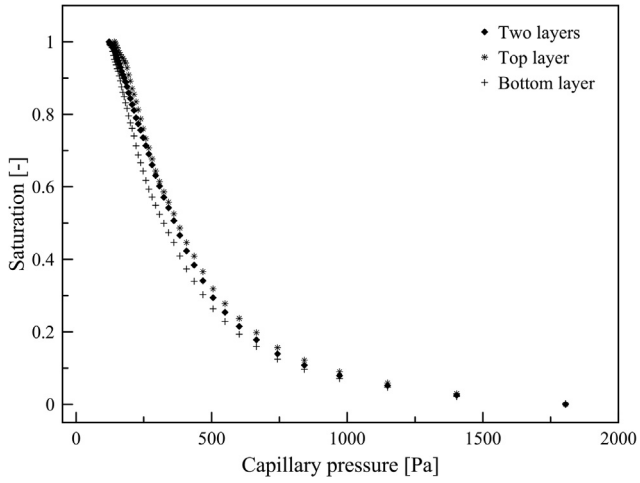

Fig. 9. Capillary pressure-saturation data obtained from pore morphology method for the top layer, the bottom layer, and the two layers of compressed polyethylene terephthalate material.

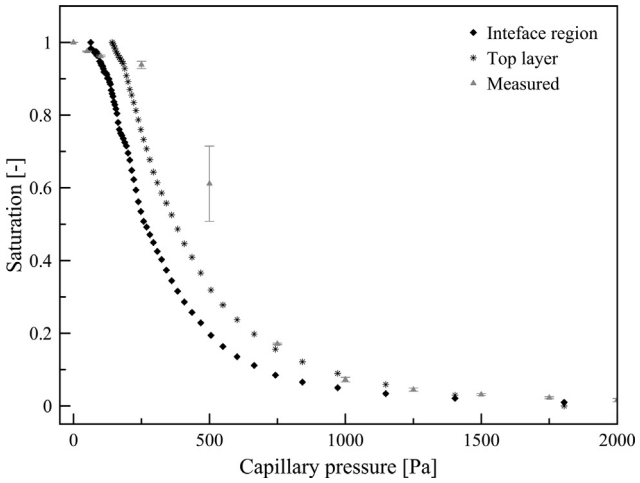

Fig. 10. Capillary pressure-saturation data computed from pore morphology method for the top layer and the interface region of a compressed stack of two polyethylene terephthalate layers. Measured data points for a single layer are shown as well.

Table 2
Properties of two polyethylene terephthalate fibrous layers used in this study obtained from simulations with Geodict software.

Parameter	Top layer	Bottom layer	Stack	Interface region
Porosity, φ [-]	0.889	0.902	0.895	0.924
K[m^2], Jackson & James	4.4e-10	5.5e-10	4.9e-10	8.3e-10
K_{xx}[m^2], Geodict	5.0e-10	7.7e-10	8.7e-10	1.8e-10
K_{zz}[m^2], Geodict	2.7e-10	3.5e-10	3.1e-10	3.03e-9
VG model,α [1/Pa]	0.0026	0.0026	0.0026	0.0043
VG model,n [-]	4	4	4	3.2
Thickness [μm]	316	316	632	44

For *model 3*, the 14 subdomains were numbered from the upper surface of the top layer to the lower surface of the bottom layer. As listed in Table B1 (Appendix B), the porosity varies non-uniformly from top to bottom. The fitted values of the α parameter in van Genuchten (VG) relationship, (which is a measure of entry pressures of subdomains), correlate with porosity variations over the subdomains. Values of intrinsic permeability of all subdomains are tabulated in Appendix B.

3. Numerical approaches

3.1. Traditional Richards model

We present equations for the traditional Richards model and the Reduced Continua Model (RCM). In this study, gravity is assumed to be negligible due to the small thickness of the layers. Thus, the Richards equation can be written as:

$$\frac{\partial(\varphi S^{w})}{\partial t} - \nabla.\left(\frac{k^{r}K}{\mu^{w}}\nabla P^{w}\right) = 0 \tag{1}$$

where φ is porosity, S^{w} is the saturation of the wetting phase, K is the intrinsic permeability, k^{r} is the relative permeability of the wetting phase, μ^{w} is the dynamic viscosity of the wetting phase, and P^{w} is the wetting phase pressure. As air phase is infinitely mobile and at constant pressure, wetting phase pressure can be linked to capillary pressure P^{c}as follows:

$$P^{w} = -P^{c}(S^{w}) \tag{2}$$

This $P^{c}(S^{w})$ and unsaturated relative permeability functions are given by the van Genuchten (1980) formulas as follows:

$$\begin{cases} P^{c}(S^{w}) = \frac{1}{\alpha}\left(S^{w-1/m} - 1\right)^{1/n} \\ k^{r}(S^{w}) = S^{w0.5}\left(1 - \left(1 - S^{w1/m}\right)^{m}\right)^{2} \end{cases} \tag{3}$$

where α and n are fitting parameters, and $m = 1 - 1/n$. Note that in this formulation, due to the very large porosity of the samples, no residual air saturation has been considered.

In this study, the Feflow software (DHI Wasy, Berlin) was used to solve Richards equation for liquid flow in a stack of two thin layers. The two-layer 3D domain was discretized in three different ways, as explained earlier in Section 3. First, in *model 1*, both sub-domains were considered to be homogeneous, corresponding to the two layers, with their properties given in Table 2. They were discretized into a mesh of 10890 hexahedral elements. Auxiliary computations showed that we had mesh-independent results. In *model 2* approach, we considered three homogeneous layers, with the 44 μm middle layer representing the interface region. In *model 3*, the two layers and their interface region were subdivided into 14 homogeneous slices, with their properties given in Table B1. A mesh of 199962 hexahedral elements was generated for this computational domain. Eqs. (1)–(3) together with the applied boundary condition were solved numerically for all above-mentioned cases using the finite element solver with standard iterative schemes.

For the traditional Richards model, the stack of two layers was simulated as a three-dimensional domain. All boundaries were considered to be no-flux boundaries except for a circular area (with diameter of 1 mm) in the middle of top surface of the upper layer, where water was introduced at a constant rate. There, a uniform liquid flow rate of 30 μl/min or 11.4 μl/min normal to the boundary was specified.

3.2. RCM approach

In RCM, all properties are averaged over the thickness and they may vary in the in-plane direction only. The mass conservation equation for water transport in layer i of a stack of layers can be written as follows:

$$\left.\frac{\partial(b\rho^{w}\varphi S^{w})}{\partial t}\right|_{i} - \nabla_{h}.\left.\left(b\rho^{w}\frac{k^{r}K}{\mu^{w}}\nabla_{h}P^{w}\right)\right|_{i} = Q_{T}^{w}|_{i} + Q_{B}^{w}|_{i} \tag{4}$$

where ρ^{w} is the mass density of the wetting phase, ∇_{h} is planar spatial gradient, $Q_{T}^{w}|_{i}$ and $Q_{B}^{w}|_{i}$ denote the influx and the outflux of water for layer *i*, respectively, and b is the layer thickness. The flux between the top and the bottom layers is assumed to be related to the difference in pressures as follows (Qin and Hassanizadeh, 2014):

$$Q_{B}^{w}|_{1} = -Q_{T}^{w}|_{2} = \Pi_{m}(P_{2}^{w} - P_{1}^{w}) \tag{5}$$

where Π_{m} is the coefficient of mass transfer between two adjacent layers. This coefficient is specific to the two neighboring layers but also accounts for the nature of contact between them. It is considered to be a function of saturations via their relative permeability.

One of the main challenges in modeling multiple layers arrangements is how to consider the effect of layer-layer interstitial space during fluid flow. This is required due to the fact that the properties of that region depend not only on its porosity but also on the fiber connectivity of two neighboring layers, particularly at low saturation. This factor can be determined considering the interpenetration of fibers, fabrics setting and fiber orientations of the two layers. The fibers connectivity, which facilitates water transport from one layer to another, is a function of external pressure applied to the layers. Moreover, the fibers direction affects fluid flow movement. For fabrics with fibers lying mainly in planar direction, chance for water exchange between the two layers is small at low saturation. Additionally, for fabrics with bonding points, the way fabrics face each other may result in different fluid flow conditions. A comprehensive sensitivity study needs to be done to evaluate the significance of each factor. Based on previous experimental results in the literature (Mohebbi et al., 2018), the saturation should build up in one layer to overcome the interlayer space resistance to water flow to the next layer. In the RCM approach, we lump all interface effects in the mass transfer coefficient Π_{m}, which is assumed to be a function of the effective permeability (i.e., product of intrinsic and relative permeabilities) of both layers. In particular, we propose the following formula:

$$\Pi_{m} = \begin{cases} 0 & S_{1}^{w} < S_{th}^{w} = 0.25 \\ \frac{2}{b_{1}+b_{2}}\rho^{w}\frac{\bar{K}_{t}}{\mu^{w}}\lambda & S_{1}^{w} > S_{th}^{w} = 0.25 \end{cases} \tag{6}$$

$$\bar{K}_{t} = \left(\frac{b_{1}+b_{2}}{b_{2}K_{1}k_{1}^{r} + b_{1}K_{2}k_{2}^{r}}K_{1}k_{1}^{r}K_{2}k_{2}^{r}\right) \tag{7}$$

Here λ is a dimensionless factor that accounts for the condition of the interface region. It varies depending on the compression.S_{th}^{w} is a local saturation threshold that should be reached in the upper layer before liquid penetration into the lower layer can start. This value was chosen to be 0.25, based on experimental observations in our earlier study (Mohebbi et al., 2018), as explained in Section 2. After conducting pathways between the two layers are established, the mass transfer coefficient is assumed to be related to the harmonic mean of effective permeabilities of the two layers weighted by their thickness, as given by Eq. (7). This empirical formula was proposed by Tavangarrad et al., (2018). As they suggested, a percolation threshold was assumed for the relative permeability function, in which the values of this function were reduced significantly in saturations below 0.25. The coefficient λ is introduced to account

for the speed of fluid exchange between the two layers and takes values between 0 and 1. As an example, our preliminary experimental result for two polyester layers without compression showed that the liquid remained in the top layer. In that experiment, $S_{th}^{w} = 1$ and $\lambda = 0$. Increasing the compression leads to a lower saturation threshold and higher λ values. For the case of 0.3 psi (≅2.1 kPa) compression on top of the two 43 gsm polyester layers, values $S_{th}^{w} = 0.25$ and $\lambda = 0.01$ were used in our simulations.

Eq. (2) and (4)–(7) were coded in COMSOL. The two layers were discretized into two 2D domains using a total of 400 tetrahedral mesh elements. Obviously, one major advantage of the RCM approach is that the computational effort is significantly reduced.

For the RCM approach, the stack of two layers was modeled as two interacting two-dimensional domains. The inlet boundary condition was specified to be the source term $Q_T^w|_1$, but of course only over a circular area of 1 mm in diameter in the middle of the top layer. Everywhere else $Q_T^w|_1$ was set equal to zero. Also, $Q_B^w|_2$ was set to zero for all (x, y) points.

4. Results and discussion

Results of 3D Richards model are averaged for each mesh layer (in the planar direction) to obtain 1D profiles along the thickness. Experimental results for the high flow rate experiment (30 μl/min) are plotted in Fig. 11, along with results of simulations of the traditional Richards equation with three different subdivision models (i.e., three different characterization approaches). We note large differences between measured and simulation results at $t = 10$ s. As the two layers are basically the same in *model 1*, the Richards model predicts the water infiltration to move as a sharp front and everywhere reaching an almost uniform low saturation in 10 s. Result of *model 3*, consisting 14 subdomains, is the only one that preserves a bell shape form similar to the experimental results. However, the water is distributed almost equally between the two layers in this model while the measurement data shows that the top layer saturation is much higher than the bottom layer saturation after 10 s.

Results of the Richards model for the high flow rate experiment (30 μl/min) at the end of fluid injection ($t = 60$ s) are shown in Fig. 12. Only *model 3* results are in relatively good agreement with the measured saturation profile for the top layer. For the bottom layer, it still shows much higher saturation than measured.

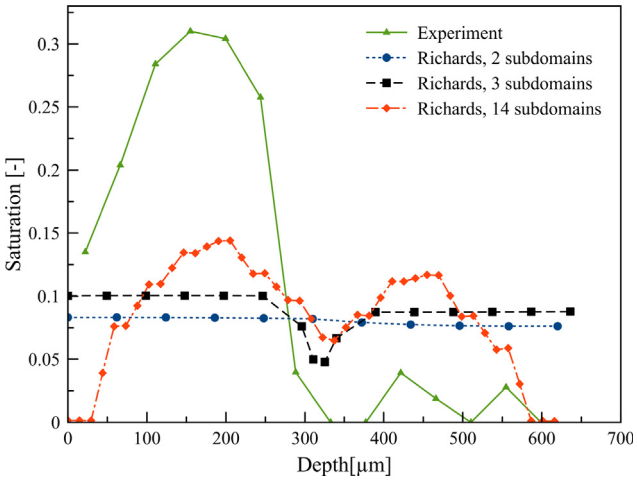

Fig. 11. Saturation profiles at $t = 10$ s across the depth of two layers, for the case of a constant flow rate of 30 μl/min. NMR measurements (in green) as well as the Richards model results are shown. (For interpretation of the references to colour in this figure legend, the reader is referred to the web version of this article.)

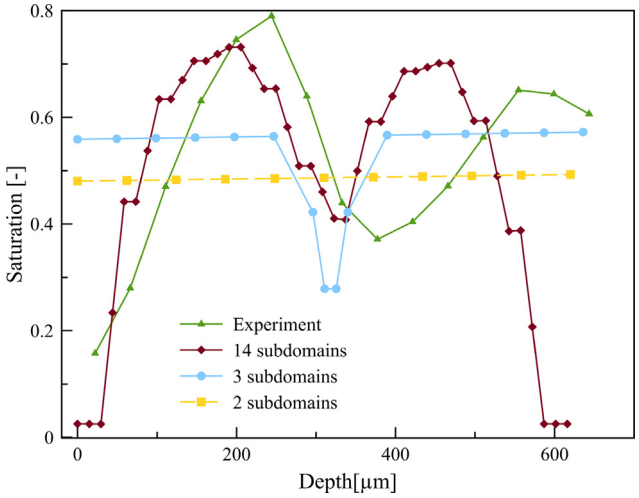

Fig. 12. Saturation profiles at $t = 60$ s over the thickness of two layers. NMR measurement and the Richards model results are compared for the case of a constant flow rate of 30 μl/min applied to the inlet boundary.

Next, we compare the modeling and experimental results for the change of the layer-averaged saturation of the top and bottom layers with time, as shown in Fig. 13. We can see that the results of the Richards model for all three characterization schemes drastically differ from the measurements. In all three cases, the average saturations of both layers start to increase as soon as the experiment starts. Even results of *model 3* (with14 subdomains) show only a marginal improvement (see Fig. 13c).

Results of the RCM for the layer-averaged saturation are compared to experimental data in Fig. 14. We can see that an excellent agreement is reached between the simulation results and the experimental data. The ability of the RCM approach for simulating the flow in a stack of two layers was further confirmed by simulating the experiment that was performed at a flow rate of 11.4 μl/min, without changing the values of the material coefficients. Results are compared to experimental data in Fig. 15. Good agreement is reached between the RCM and the experimental results, as the main features of the experimental data are reproduced by RCM. The time lag for the water infiltration into the lower layer is larger for this low flow-rate experiment.

Another advantage of RCM approach is that the computational time was about one order of magnitude less than that of the Richards model. While the CPU time for the Richards model considering two homogenous domains was 1480 ± 458 s, RCM needed a 190 ± 42 s. At the same time, it must be noted that the spatial variation of saturation along the thickness of layers cannot be given by RCM, as it is formulated in terms of the layered-averaged saturation.

At high compression, even though the interface region cannot be distinguished from the two layers, there still exist discontinuities of fibers in the interface region. Therefore, a comprehensive study is needed to assess the effect of fiber discontinuity on liquid exchange between thin layers. This is particularly important at low saturation, where the extruding fibers play a significant role in delivering liquid from one layer to the other one. Even in that case, if fibers are not distributed uniformly across a layer thickness, the layer cannot be treated as one homogeneous domain in Richards model in order to obtain liquid distribution across the thickness of the layer. Obviously for cases that layers are thick, Richards model can be reliably used for simulations. It is of course necessary

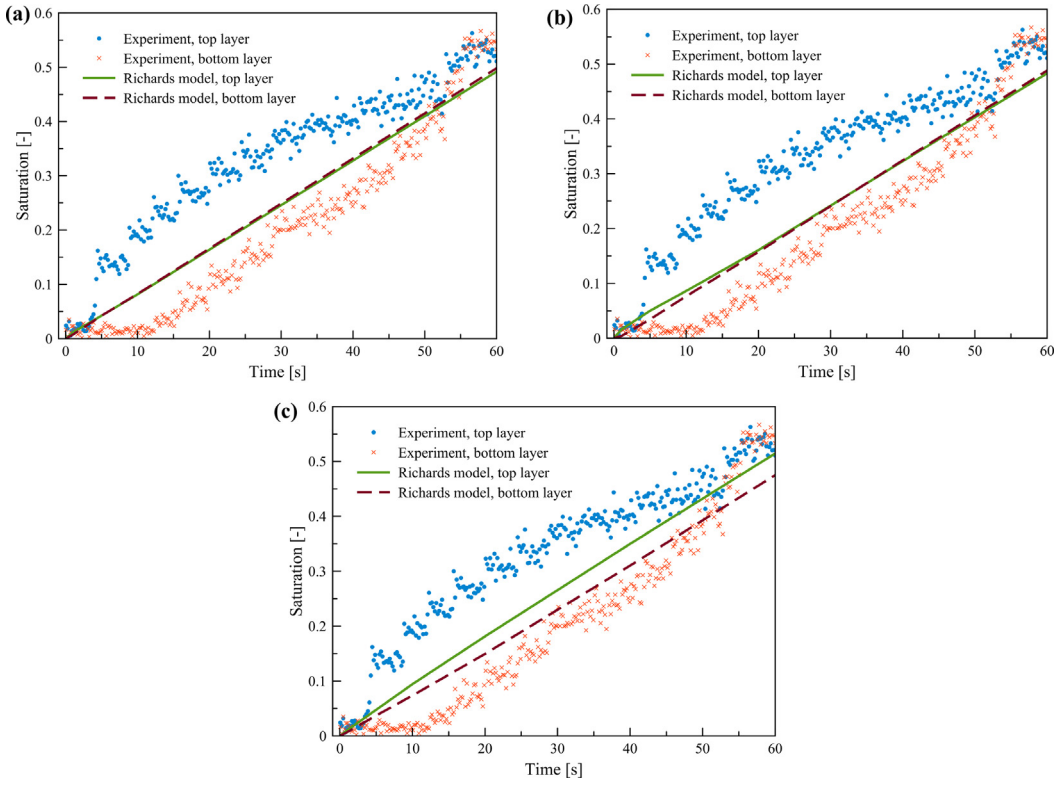

Fig. 13. Comparison of temporal evolution of the layer-averaged saturation of each layer over time obtained from NMR measurements with results of the Richards model with three different characterization approaches: (a) two homogeneous subdomains (*model 1*), (b) three homogeneous subdomains (*model 2*, with the middle domain representing the interface region), (c) fourteen homogeneous subdomains (*model 3*).

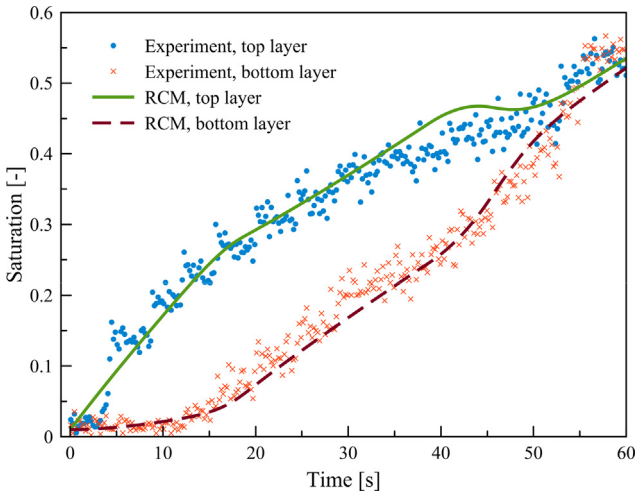

Fig. 14. Comparison of the temporal evolution of the layer-averaged saturation in a stack of two thin layers obtained from NMR measurements and the Reduced Continua Model in the experiment with a constant flow rate of 30 μl/min.

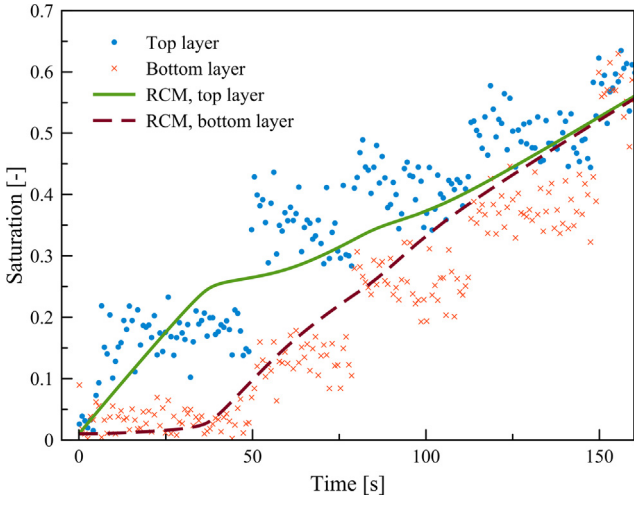

Fig. 15. Comparison of the temporal evolution of the layer-averaged saturation in a stack of two thin layers obtained from NMR measurements and the Reduced Continua Model in the experiment with a constant flow rate of 11.4 μl/min.

to further investigate the effect of different interfaces and boundary conditions for unsaturated fluid flow in thin fibrous layers. We are working now on the study of one-step inflow/outflow experiments to evaluate effects of thin layers roughness and contact between the two thin layers on non-equilibrium conditions.

This study evidenced the role of the interface on impeding the water transport across two thin layers, which is reproduced in the RCM numerical solution by implementing the saturation buildup threshold and the λ coefficient in the mass transfer coefficient. Imperfect contact was included in an exchange coefficient by setting $\lambda = 0.01$. This value works perfectly for the current layer-layer setting for different inlet boundary flow rates.

5. Conclusions

In this study, water infiltration into a stack of two thin fibrous layers is investigated numerically. The traditional Richards model and the Reduced Continua Model are employed to simulate the temporal evolution of the saturation. Results are compared to experimental data.

Traditional Richards model results cannot reproduce saturation distribution profiles along the thickness when the measured average properties are assigned to a layer. More importantly, delayed water movement due to the presence of inter-layer space cannot be simulated using the traditional Richards model. However, in the RCM, the effect of an inter-layer space is embedded in a mass transfer coefficient. This feature enabled RCM to reproduce results of two different experiments performed under different boundary conditions. The results of this research proves the superiority of the RCM in simulating through-plane infiltration across a stack of thin fibrous layers to the traditional Richards model in terms of both accounting for the layer-layer mass exchange effect and the computational effort.

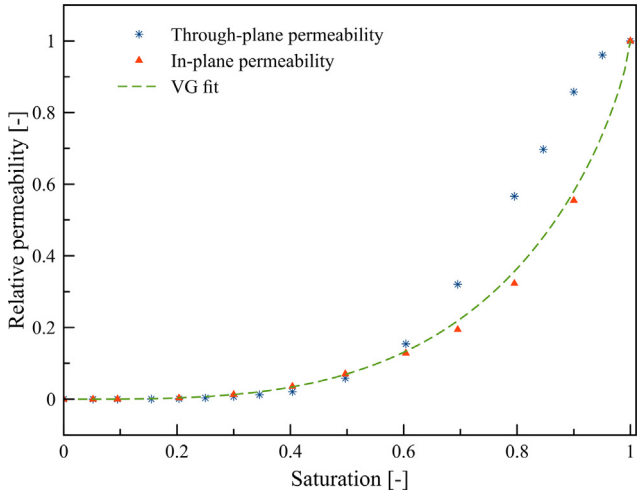

Fig. A1. Relative permeability data points obtained from the pore morphology method combined with the Stokes equation for a compressed polyethylene terephthalate layer. The VG-fit curve is based on the Muallem-van Genuchten formula and the resulting fit parameters appear in the capillary pressure saturation relationship.

Declaration of Competing Interest

The authors declare that they have no known competing financial interests or personal relationships that could have appeared to influence the work reported in this paper.

Acknowledgement

The research leading to these results has received funding from the European Research Council under the European Union's Seventh Framework Program (FP/2007-2013)/ERC Grant Agreement no. 341225 and from Procter & Gamble.

Appendix A. Relative permeability function of a thin fibrous layer using pore morphology method and van Genuchten fitting parameters

To find the relative permeability function, we first implemented the pore morphology method to obtain the wetting phase distribution for each capillary pressure. Then, a single-phase simulation was run by solving the Stokes equation in the voxels occupied by the wetting phase using Geodict. The relative permeability data points obtained by this approach are compared with the Muallem-van Genuchten function, which is calculated based on the parameters appearing in the $P^c(S^w)$ relationship. As shown in Fig. A1, good agreement was achieved between the Geodict results and the estimated VG function. Although the results of the capillary pressure-saturation for a single 43-gsm layer did not depend on the flow direction, the relative permeability function varies from the in-plane to the through-plane directions. However, this discrepancy had negligible effect on the final simulation results. Therefore, we decided to consider the VG formula for the relative permeability in Eq. (3) for all of the modeling case studies in this work.

Appendix B. Properties of 14 subdomains of two polyester layers

The properties of the subdomains of *model 3* are listed in the following table (see Table B1).

Table B1
The properties of the different 44-μm thick subdomains of two polyethylene terephthalate fibrous layers used in this study.

# Domain	Porosity [-]	K [m^2] Jackson & James	Kxx[m^2] Geodict	Kzz[m^2] Geodict	VG formula α[1/Pa]	VG formulan[-]
1	0.97	4.9e-09	4.9e-9	2.9e-8	0.0144	3.2
2	0.91	6.9e-10	1.7e-10	2.9e-9	0.0043	2.7
3	0.87	3.2e-10	7.8e-11	1.3e-9	0.0027	2.9
4	0.85	2.4e-10	5.6e-11	6.9e-10	0.0024	2.9
5	0.84	2.2e-10	5.6e-11	8e-10	0.0023	2.9
6	0.86	3.0e-10	7.3e-11	1.4e-9	0.0027	2.9
7	0.90	5.5e-10	1.4e-10	3.5e-9	0.004	2.7
8	0.92	7.8e-10	1.8e-10	2.4e-9	0.0045	2.7
9	0.87	3.6e-10	8.3e-11	1.4e-9	0.0034	2.7
10	0.85	2.6e-10	5.8e-11	7.3e-10	0.0034	2.7
11	0.85	2.4e-10	5.3e-11	8e-10	0.0026	2.9
12	0.88	3.6e-10	7.9e-11	1.4e-9	0.0029	2.9
13	0.93	8.6e-10	2e-10	5.1e-9	0.0048	2.7
14	0.98	5.2e-09	4.4e-9	2.8e-8	0.0144	3.2

References

Albrecht, W., Fuchs, H., Kittelmann, W., 2003. Non-woven fabrics: raw materials, manufacture, applications, characteristics, testing processes. Wiley.

Birrfelder, P., Dorrestijn, M., Roth, C., Rossi, R.M., Sarkar, M.K., 2013. Effect of fiber count and knit structure on intra- and inter-yarn transport of liquid water. Text. Res. J. 83 (14), 1477–1488.

Carrere, P., Prat, M., 2019. Liquid water in cathode gas diffusion layers of PEM fuel cells: identification of various pore filling regimes from pore network simulations. Int. J. Heat Mass Transf. 129, 1043–1056. https://doi.org/10.1016/j.ijheatmasstransfer.2018.10.004.

Diersch, H.J.G., Clausnitzer, V., Myrnyy, V., Rosati, R., Schmidt, M., Beruda, H., Ehrnsperger, B.J., Virgilio, R., 2011. Modeling unsaturated flow in absorbent swelling porous media: Part 2. numerical simulation. Trans. Porous Media 86 (3).

Hao, L., Moriyama, K., Gu, W., Wang, C.-Y., 2016. three dimensional computations and experimental comparisons for a large-scale proton exchange membrane fuel cell. J. Electrochem. Soc. 163 (7).

Hazlett, R.D., 1995. Simulation of capillary-dominated displacements in microtomographic images of reservoir rocks. Trans. Porous Media 20–21.

Hilpert, M., Miller, C.T., 2001. Pore-morphology-based simulation of drainage in totally wetting porous media. Adv. Water Resour. 24 (3/4), 243–255.

Hizir, F.E., Ural, S.O., Kumbur, E.C., Mench, M.M., 2010. Characterization of interfacial morphology in polymer electrolyte fuel cells: Micro-porous layer and catalyst layer surfaces. J. Power Sour. 195 (11), 3463–3471.

Jackson, G.W., James, D.G., 1986. The permeability of fibrous porous media. Can. J. Chem. Eng. 64, 362–374.

Garcia-Salaberri, P.A., Zenyuk, I.V., Shum, A.D., Hwang, G., Vera, M., Weber, A.Z., Gostick, J.T., 2019. Analysis of representative elementary volume and through-plane regional characteristics of carbon-fiber papers: diffusivity, permeability and electrical/thermal conductivity. Int. J. Heat Mass Transf. 127, 687–703.

Leisen, J., Beckham, H.W., 2009. Fluid distribution and movement in engineered fibrous substrates by magnetic resonance microscopy magnetic resonance microscopy: spatially resolved NMR techniques and applications. Wiley-VCH Weinheim.

Miller, B., Tyomkin, I., 1994. Liquid porosimetry: new methodology and applications. J Col Int Sci. 62, 163–170.

Mohebbi, B., Tavangarrad, A.H., Clausen, J., Blümich, B., Hassanizadeh, S.M., Rosati, R., 2018. Revealing how interfaces in stacked thin fibrous layers affect liquid ingress and transport properties by single-sided NMR. J. Mag. Resonance 294, 16–23.

Mohebbi, B., Clausen, J., Blümich, B., 2019. Fast and robust quantification of liquid inside thin fibrous porous materials with single-sided NMR. J Magn Reson Imaging.

Prat, M., Agaësse, T., 2015. Thin porous media. In: Vafai, K. (Ed.), Handbook of Porous Media (Chapter 4). 3rd ed. Taylor & Francis, London.

Qin, C.Z., Hassanizadeh, S.M., 2014. Multiphase flow through multilayers of thin porous media: general balance equations and constitutive relationships for a solid-gas-liquid three-phase system. Int. J. Heat Mass Transf 70, 693–708.

Qin, C.Z., Hassanizadeh, S.M., 2015. A new approach to modelling water flooding in a polymer electrolyte fuel cell. Int. J. Hydrogen Energy 40, 3348–3358.

Qin, C., Guo, B., Celia, M., Wu, R., 2019. Dynamic pore-network modeling of air-water flow through thin porous layers. Chem Eng Sci.

Sweijen, T., Aslannejad, H., Hassanizadeh, S.M., 2017. Capillary pressure-saturation relationships for porous granular materials: pore morphology method vs. pore unit assembly method. Adv. Water Resour. 107, 22–31.

Tafreshi, H.V., Bucher, T.M., 2013. Modeling fluid absorption in anisotropic fibrous porous media. In: Masoodi, R., Pillai, K.M. (Eds.), Wicking in Porous Materials. CRC Press, Boca Raton, pp. 131–159.

Tavangarrad, A.H., Mohebbi, B., Hassanizadeh, S.M., Rosati, R., Clausen, J., Blümich, B., 2018. Continuum-scale modeling of liquid redistribution in a stack of thin hydrophilic fibrous layers. Trans. Porous Media. 122, 203–219.

Tavangarrad, A.H., Hassanizadeh, S.M., Rosati, R., Digirolamo, L., van Genuchten, M.T., 2019. Capillary pressure–saturation curves of thin hydrophilic fibrous layers: effects of overburden pressure, number of layers, and multiple imbibition–drainage cycles. Text. Res. J. https://doi.org/10.1177/0040517519844209.

Tavangarrad, A.H., 2019. Experimental and computational study of unsaturated flow in a stack of thin layers, application to non-woven hygiene products PhD Thesis. Utrecht University.

Van Genuchten, M.Th., 1980. A closed-form equation for predicting the hydraulic conductivity of unsaturated soils. Soil Sci Soc. Am J. 44, 892–898.

Zhuang, Q., Harlock, S.C., Brook, B.D., 2002. Transfer wicking mechanisms of knitted fabrics used as undergarments for outdoor activities. Textile. Res. J. 72 (8), 727–734.